Combined adsorption and oxidation mechanisms of hydrogen sulfide on granulated coal ash

Asaoka, Satoshi ; Hayakawa, Shinjiro ; Kim, Kyung-Hoi ; Takeda, Kazuhiko ; Katayama, Misaki ; Yamamoto, Tamiji

(Citation)
Journal of Colloid and Interface Science,377(1):284-290

(Issue Date)
2012-07-01

(Resource Type)
journal article

(Version)
Accepted Manuscript

(URL)
https://hdl.handle.net/20.500.14094/90003331

Combined adsorption and oxidation mechanisms of hydrogen sulfide on granulated coal ash

Satoshi ASAOKA[a*], Shinjiro HAYAKAWA[b], Kyung-Hoi KIM[c], Kazuhiko TAKEDA[c], Misaki KATAYAMA[d], Tamiji YAMAMOTO[c]

[a] 1-5-3 Kagamiyama, Higashi-Hiroshima, Hiroshima, Japan 739-8513

[b] 1-4-1 Kagamiyama, Higashi-Hiroshima, Hiroshima, Japan 739-8527

[c] 1-4-4 Kagamiyama, Higashi-Hiroshima, Hiroshima, Japan 739-8528

[d] 1-1-1 Nojihigashi, Kusatsu, Shiga, Japan 525-8577

[a] Environmental Research and Management Center, Hiroshima University

[b] Graduate School of Engineering, Hiroshima University

[c] Graduate School of Biosphere Science, Hiroshima University

[d] Ritsumeikan University SR Center, Ritsumeikan University

*Corresponding author

Tel: +81-82-424-7622

Fax: +81-82-424-4351

E-mail address: st-asaoka@hiroshima-u.ac.jp

Address: Environmental Research and Management Center, Hiroshima University, 1-5-3 Kagamiyama, Higashi-Hiroshima, Japan 739-8513

Abstract

Hydrogen sulfide is highly toxic to benthic organisms and may cause blue tide with depletion of dissolved oxygen in water column due to its oxidation. The purpose of this study is to reveal the combined adsorption and oxidation mechanisms of hydrogen sulfide on granulated coal ash which is a byproduct from coal electric power stations to apply the material as an adsorbent for hydrogen sulfide in natural fields. Sulfur species were identified in both liquid and solid phases to discuss removal mechanisms of the hydrogen sulfide with the granulated coal ash. Batch experiments revealed that hydrogen sulfide decreased significantly by addition of the granulated coal ash and simultaneously the sulfate ion concentration increased. X-ray absorption fine structure analyses showed hydrogen sulfide was adsorbed onto the granulated coal ash and successively oxidized by manganese oxide (III) contained in the material. The oxidation reaction of hydrogen sulfide was coupling with reduction of manganese oxide. On the other hand, iron containing in the granulated coal ash was not involved in hydrogen sulfide oxidation, because the major species of iron in the granulated coal ash was ferrous iron which is not easily reduced by hydrogen sulfide.

Key words

coal ash, enclosed water body, manganese, iron, sediment, X-ray absorption fine structure

1. Introduction

Generally, the sediments lying under enclosed water bodies adjacent to large metropolis are affected by high organic sedimentation fluxes from terrigenous loads and internal cycles attributed to primary production. Organic matter retained on the bottom of enclosed water bodies consumes large amount of dissolved oxygen from the water column through its oxidative decomposition processes. Hypoxic water mass is often formed during the stratified seasons. Under such reduced condition, hydrogen sulfide that is highly toxic to benthic organisms is generated through sulfate reduction by sulfate reducing bacteria. It may also cause depletion of dissolved oxygen in the bottom water due to its oxidation resulting to the deterioration of benthic ecosystems. Since oxygen depletion is fatal to organisms, it sometimes brings much economic losses to aquaculture activities. Therefore, it is very important to reduce the concentration of hydrogen sulfide in sediments so as to maintain healthy ecosystems and provide sustainable aquaculture activities.

Removal or adsorption strategies of hydrogen sulfide are mainly catalytic oxidation [1-4] or formation of sulfide [5, 6]. Some metals act as efficient catalysts for hydrogen sulfide oxidation, such as Na_2CO_3 impregnated coal-based activated carbon [1], bismuth-molybdenum binary oxides [2], Fe/MgO nano-crystals [3], and vanadia–titania aerogel [4]. It was also reported that iron, zinc, and copper species play important roles in the formation of sulfide [5, 6].

Granulated coal ash (GCA) is a by-product generated from coal combustion processes in coal thermal electric power stations. In 2007, twelve mega tons of coal ash were generated from coal thermal electric power stations and other industries in Japan [7]. Previous studies have proven that GCA

adsorbed effectively hydrogen sulfide in seawater [8]. Accordingly, in container experiments designed for simulating enclosed water bodies, the concentration of hydrogen sulfide in pore water of organically enriched marine sediment mixed together with GCA decreased significantly by 77-100% compared to those without application of GCA [9]. Remarkably, the GCA has quite a high adsorption capacity, 108 mg-S g^{-1} for hydrogen sulfide compared to other materials [8]. The assumed removal processes of hydrogen sulfide by GCA are the formation of sulfide with trace or sub-trace element contained in GCA and oxidation [8]. However, the exact hydrogen sulfide removal mechanism, namely, elements which have contributed towards hydrogen sulfide oxidation reaction is not fully understood. The purpose of this study is to reveal the combined adsorption and oxidation mechanisms of hydrogen sulfide occurring at the surface of GCA.

2. Materials and methods

2.1. Granulated coal ash (GCA)

The GCA tested in this study is a commercially sold product, named "Hi-beads" (Energia Eco Materia Co., Inc.) with 5 mm diameter, which is produced through the granulation process of pulverized fly ash from coal firing systems in thermal electric power stations (Chugoku Electric Power) with added cement as binder amounting to 10-15% of the final product. The GCA is mainly composed of SiO_2, CO_3^{2-}, Al_2O_3, CaO, C and Fe_2O_3 with quartz and aluminosilicate crystal phase, and their concentrations are 395, 133, 126, 55.4, 27.4 and 22.5 g kg^{-1}, respectively (Table1). TiO_2 and MnO contents are 5.68 g kg^{-1} and 329 mg kg^{-1}, respectively [10]. The environmentally regulated substances dissolved from the GCA used in this study were obviously below the standard levels for environmental criteria in Japan [10].

2.2. Adsorption experiment

Adsorption experiment was carried out in a 100 mL BOD bottle containing 50 mL of the hydrogen sulfide solution with concentrations of 8 and 85 mg-S L^{-1} which represents possible levels in the pore water of organically enriched marine sediments. The hydrogen sulfide solution was prepared as follows: aliquot of $Na_2S \cdot 9H_2O$ (Nacalai Tesque) was dissolved in 500 mL pure water deaerated with N_2 gas. Thereafter, the pH of the solution was adjusted to 8.2 with HCl. Fifty mL of hydrogen sulfide solution was slowly dispensed into the bottle and 0.2 g of the GCA was added to the solution. The amount of GCA is optimized on the basis of the previous study to minimize change of pH [8]. Thereafter, the head space of the bottle was replaced with N_2 gas and capped tightly using grease for vacuum use. The bottle was agitated moderately at 100 rpm at 25 ^oC in a water bath, and time courses of hydrogen sulfide concentration, pH, and oxidation reduction potential (ORP) were measured with a detection tube (200SA or 200SB: Komyo Rikagaku Kougyo), pH electrode (F-22: Horiba Ltd.), and ORP electrode (RM-20P: DKK-TOA Co.), respectively. The ORP value was converted to Eh value following standard methods [11].

To quantify the sulfur mass balances, sulfate ion concentration was also determined after scavenging remaining hydrogen sulfide with formation of ZnS so as to prevent further oxidation of hydrogen sulfide during analysis. The procedure for scavenging hydrogen sulfide was partially modified based on the Ref. [12]. Briefly, 1 mol L^{-1} of $Zn(CH_3COO)_2 \cdot 2H_2O$ solution (0.1 mL) and 6 mol L^{-1} NaOH solution (0.1 mL) were successively added to 10 mL of sample. After precipitation of ZnS, the supernatant solution was filtered through a hydrophilic PVDF filter with 0.45 μm pore size (MILLEX:

Millipore). Thereafter, pH of the filtrates was adjusted to neutral while the concentration of sulfite ion was determined using an ion chromatograph (DX-120: DIONEX) attached with an anion exchange column (Ion Pac AS12A: DIONEX). According to a pretest, the sulfate ion was perfectly recovered (98%) using this proposed method.

An experiment without GCA was also conducted as the control following the same procedure to compensate for hydrogen sulfide loss due to volatilization. These same settings were prepared in triplicates. The GCA treated in 85 mg-S L^{-1} of hydrogen sulfide solution was submitted to XAFS analyses described below.

2.3. X-ray absorption fine structure (XAFS) analyses and data processing

Sulfur and titanium K-edge XAFS spectra (ranges 2460-2485 eV for sulfur and 4950-5030 eV for titanium) were measured using the BL11 in Hiroshima Synchrotron Research Center, HiSOR [13]. The synchrotron radiation from a bending magnet was monochromatized with a Si(111) double-crystal monochromator. The sample chamber was filled with He gas, and XAFS spectra were measured both by the X-ray fluorescence yield (XFY) mode using a SDD detector (XR-100SDD; AMPTEK) and conversion electron yield (CEY) mode. The X-ray energies around K-edges of sulfur and titanium were calibrated with the spectra of $CuSO_4$ and Ti foil obtained with the CEY mode, respectively. The K-edge main peak of sulfate was set to 2481.6 eV [14] and the pre-edge peak of Ti foil of K shell was set to 4970.0 eV, respectively. As references, Na_2SO_4 (Wako Pure Chemical Industry), Na_2SO_3 (Wako Pure Chemical Industry), FeS_2 (Stream Chemicals), FeS (Wako Pure Chemical Industry), Al_2S_3, (Sigma-Aldrich), TiS_3 (Alfa Aesar), MnS (Sigma-Aldrich), CaS (Sigma-Aldrich), Ti foil (Nilako) were measured by the CEY mode. The

pieces of relatively flat GCA samples were mounted on a double-stick tape (NW-K15; Nichiban) placed in the central hole (15 mm in diameter) of a copper plate. The surface of the sample was attached to that of the copper plate. The angle between the incident X-ray and the sample surface was adjusted at 20° and the X-ray fluorescence was detected from the direction normal to the incident beam in the plane of electron orbit of the storage ring.

Manganese and iron K-edge XAFS spectra (range 6400-6725 eV for manganese and range 7080-7250 eV for Iron) were measured in BL3 st the Ritsumeikan SR center, Japan. The synchrotron radiation was monochromatized with a Si(220) double-crystal monochromator. The sample XAFS spectra were measured by X-ray fluorescence yield mode using a three-elements Ge solid state detector, SSD (GUL0110S: Canberra). Samples were sealed with polypropylene film and they were positioned at 45° to the incident beam in fluorescence mode. The X-ray energy was calibrated by defining the K edge pre-edge peak of δ-MnO_2 and hematite fixed at 6540 and 7112 eV, respectively.

For manganese standard, δ-MnO_2 (Wako Pure Chemical Industry), Mn_2O_3 (Sigma-Aldrich), $MnSO_4 \cdot 5H_2O$ (Wako Pure Chemical Industry) and MnS (Sigma-Aldrich), and for iron standard, hematite (Stream Chemicals), iron hydroxide (III) (Alfa Aesar), FeS_2 (Stream Chemicals), FeO (Alfa Aesar), FeS (Wako Pure Chemical Industry), $FeSO_4 \cdot 7H_2O$ (Wako Pure Chemical Industry) and iron foil (Alfa Aesar) were also measured by the transmission mode using an ionization chamber filled with mixed gases: Ar 15% and N_2 85% and for incident chamber (I_0) and Ar 50% and N_2 50% for transmitted chamber (I).

The spectra obtained by these XAFS analyses were processed with XAFS spectra processing software (REX2000 ver. 2.5: Rigaku co. Ltd.). Absorption

edge (E_o) was defined as the inflection point in the spectrum.

Eh-pH diagram of manganese and iron in the presence of sulfite ion was illustrated by the geochemical modeling software, Geochemist's Workbench 8.0 (RockWare). The parameters used in this thermodynamic calculation were as follows: the activities were referred to liquid phase concentration and set to be 10^{-6} mol L^{-1} for Fe^{2+}, 10^{-7} mol L^{-1} for Mn^{2+} and 10^{-3} mol L^{-1} for SO_4^{2-}. The pressure and temperature were set at 1.013 hPa and 25 ^oC, respectively. Iron and manganese concentrations in the liquid phases were measured to illustrate Eh-pH diagram using an ICP-AES (Optima 7300DV: PerkinElmer) after being filtrated through a 0.45 μm hydrophilic PVDF filter (MILLEX: Millipore) and added with HNO_3 to make 2%.

3. Results and discussion

3.1 Removal of hydrogen sulfide from liquid phase

The concentrations of hydrogen sulfide decreased significantly with the GCA compared to those of control without the GCA under both initial concentrations at 8 and 85 mg-S L^{-1} (250 and 2,660 μmol L^{-1}), respectively. After 3 or 7 d, those concentrations decreased to <3 and 220 μmol L^{-1} from 250 and 2,660 μmol L^{-1} of the initial concentrations, respectively (**Fig. 1**). On the other hand, the concentration of sulfate ion increased in the experiments with the GCA compared to those in the control (**Fig. 1**). The sulfate ion concentration of the GCA shown in **Fig 1** was calculated by subtracting the concentration of sulfate ion dissolved from the GCA itself. However, the increase of sulfate ion in the GCA was obviously higher than those in the control.

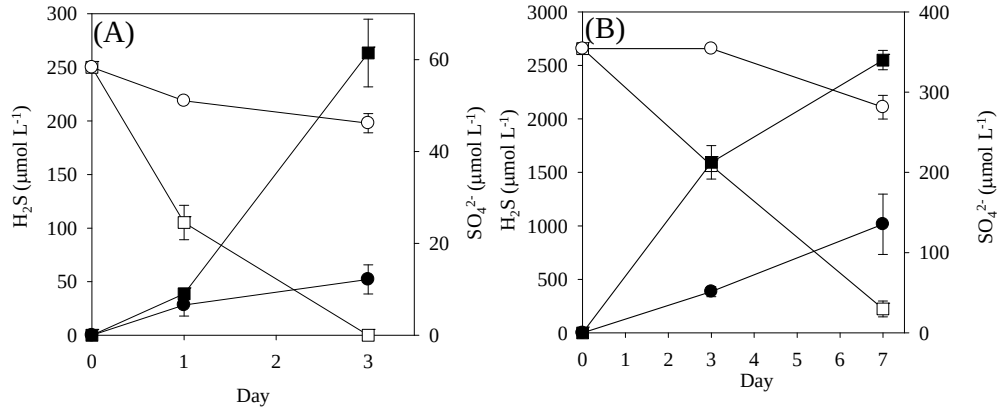

Fig. 1

The values of pH ranged between 7.6-8.3 and 8.3-9.2 for control and the GCA, respectively, under the initial concentration of 8 mg-S L^{-1} (**Fig. 2A**). With an initial concentration of 85 mg-S L^{-1}, the pH changed in the range of 6.9-8.2 in the control and 7.8-8.3 in the GCA (**Fig. 2B**). The pH with GCA was slightly higher than that of the control. The pH increase with the GCA was due to the hydrolysis of calcium dissolved from GCA as reported previously [10].

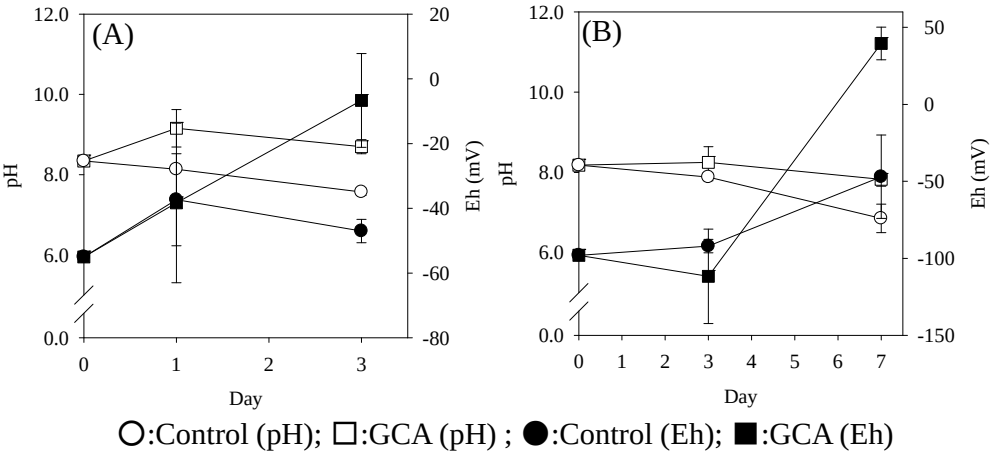

Fig. 2

The values of Eh in the GCA increased from -55 to -7 mV in the initial concentration of 8 mg-S L^{-1} and from -98 to +40 mV in the initial concentration of 85 mg-S L^{-1}, while those in the control changed only from -55 to -47 mV and from -98 to -47 mV, respectively (**Figs. 2 A and B**). The final Eh values in the GCA were higher than those in the control, which can be attributed to the removal of hydrogen sulfide.

The contributions of sulfur removal were shown in **Fig. 3**. The adsorption to solid phase was defined as in equation (1).

$$[\text{Adsorption}]=[H_2S\text{-}S]_i - \{[H_2S\text{-}S]_t + [SO_4^{2-}\text{-}S]_t + [\text{Loss-}S]_t\} \cdots (1)$$

[Adsorption], $[H_2S\text{-}S]_i$, $[H_2S\text{-}S]_t$, $[SO_4^{2-}\text{-}S]_t$ and $[\text{Loss-}S]_t$ were the amount of (mg-S) adsorbed to solid phase, H_2S-S at initial (mg-S), H_2S-S at time t (mg-S), SO_4^{2-}-S at time t (mg-S) and Loss of H_2S at time t (mg-S), respectively. Here, the Loss of H_2S at time t was calculated from the blank test without GCA, namely, by subtracting the amount of H_2S-S at time t without GCA from the H_2S-S at initial.

In the experiments with the GCA with an initial concentration of 8 mg-S L^{-1}, 25% of the hydrogen sulfide was oxidized to sulfate, 59% was adsorbed onto the GCA, and the others might be transformed to other sulfur species at Day 3 (**Fig. 3A**), while 80% of hydrogen sulfide remained in the control. With 85 mg-S L^{-1} as initial concentration, about 13% of hydrogen sulfide was oxidized to sulfate, 63% was adsorbed onto GCA and 8% remained in liquid phase and 16% was the others at Day7 (**Fig. 3B**). Thus, the hydrogen sulfide was mainly removed by adsorption onto GCA.

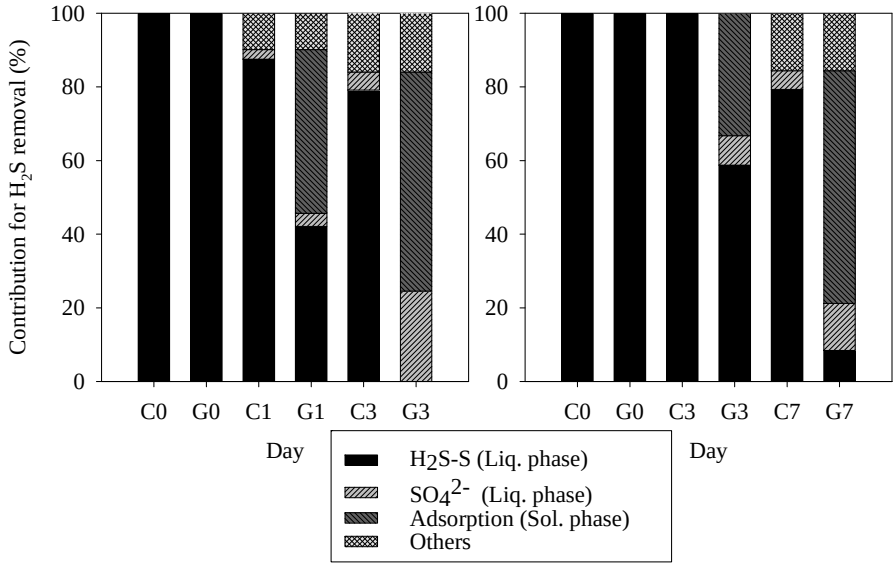

Fig. 3

3.2. Revealing adsorption mechanism of hydrogen sulfide onto the GCA using X-ray absorption fine structure analyses

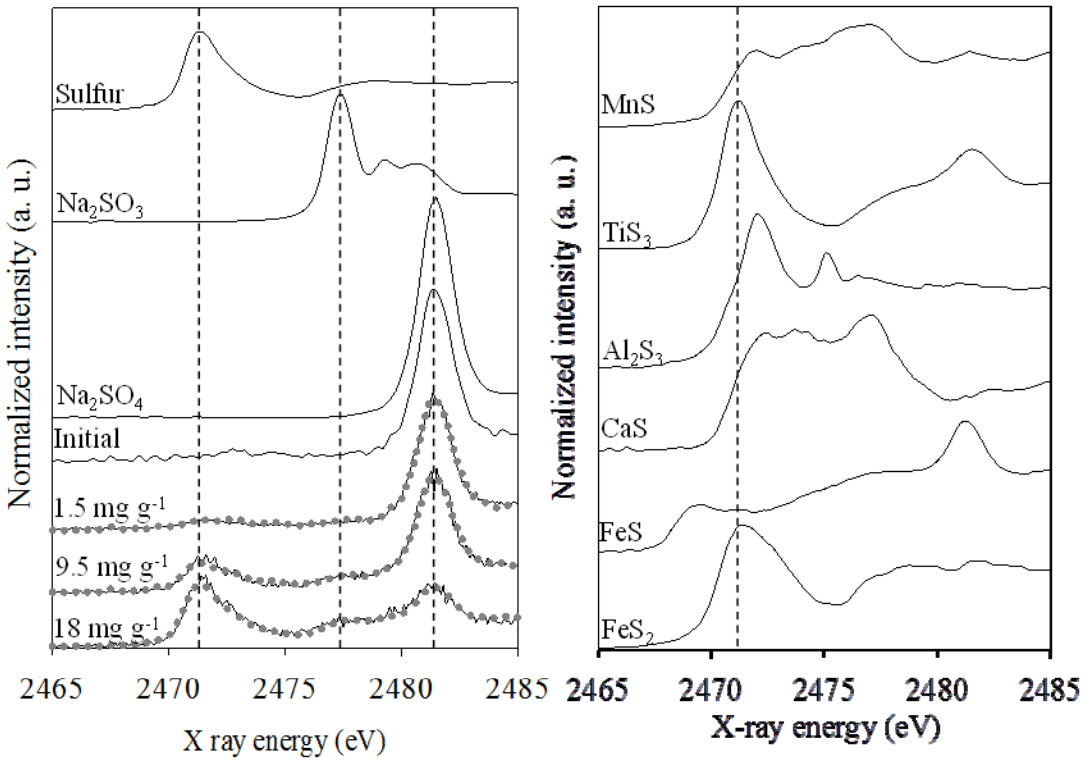

Fig. 4

In the previous study, we assumed that the removal processes of hydrogen sulfide by the GCA mainly involved the formation of sulfide with trace or sub-trace element contained in the GCA and oxidation [8]. In this study, the sulfur K edge XANES spectra with different adsorption amounts of hydrogen sulfide were measured (**Fig. 4**). The standard spectra of sulfur species, sulfide of several elements and curve fitting results were also shown in **Fig. 4**. The GCA has a peak at 2482 eV regardless of hydrogen sulfide adsorption. The peak at 2482 eV indicates sulfate which may be derived from coals [15]. New peaks were observed after hydrogen sulfide adsorption at 2472 and 2476-2478 eV. The peak at 2472 eV is quite similar to that of sulfur, which can be supported by the fact that the sulfur K edge has a peak at 2472 eV

[16]. The peak area at 2472 eV increased by the increase of hydrogen sulfide adsorption. The peak at 2476-2478 eV corresponds well with sulfite. The curve fitting results of sulfur species are discussed later. Although the sulfur peak was quite similar to the hydrogen sulfide adsorbed unto the GCA (final GCA) as compared to the standards, the MnS, TiS_3 and FeS_2 have also main peaks at around 2472 eV (**Fig. 4**). On the other hand, the main peaks of CaS, FeS, and Al_2S_3 were not comparable with that of the final GCA. Therefore, it can be assumed that hydrogen sulfide is removed by the oxidation or formation of sulfide with manganese, titanium and iron.

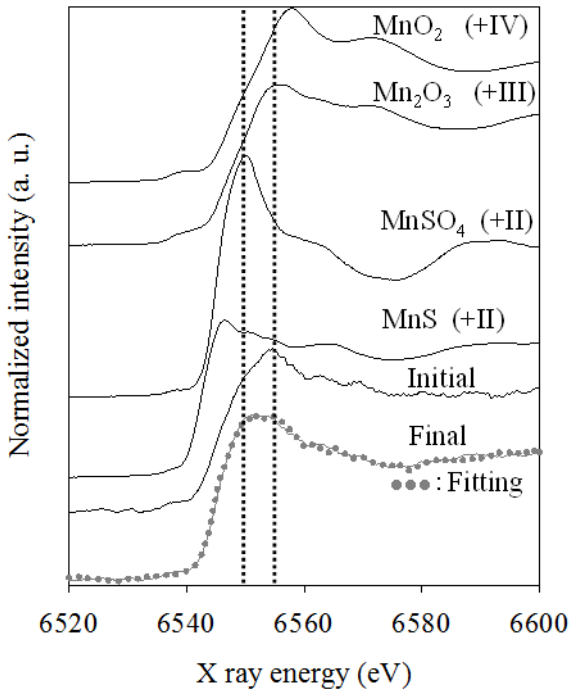

Fig. 5

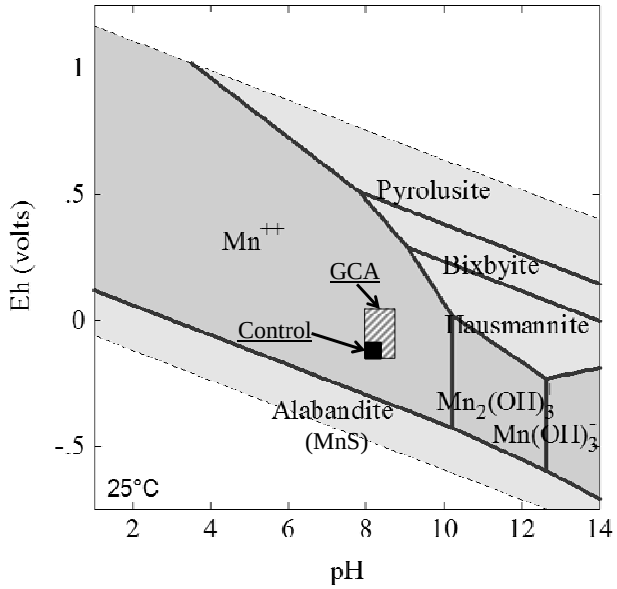

Fig. 6

Manganese, titanium and iron K edge XANES spectra were measured in order to confirm whether or not the MnS, TiS_3 and FeS_2 were formed on the surface of the GCA. The manganese K edge peak of the GCA was initially at 6554 eV and corresponded well with Mn_2O_3 indicating that the major manganese species in the GCA was trivalent, while the peak shifted to 6551 eV after adsorption of hydrogen sulfide, which coincided well with $MnSO_4$ (**Fig. 5**). On the other hand, the manganese K edge XANES of final GCA did not compare with MnS (**Fig. 5**). According to the Eh-pH diagram of manganese, MnS is considered to be thermodynamically formed under much lower redox conditions compared to those of this study (**Fig. 6**). Therefore, the manganese contained in the GCA did not form MnS under these experimental conditions. Curve fitting was conducted using $MnSO_4$ and initial GCA K edge XANES spectra to fit to that of the final GCA. The dotted curve in **Fig. 5** is the fitted curve which simulated well with the observed

XANES of the final GCA composed of 70% initial GCA and 30% $MnSO_4$, showing that the fraction of $MnSO_4$ in the final GCA increased compared to the initial GCA. Consequently, it can be said that the hydrogen sulfide was oxidized to sulfate by coupling with manganese reduction on the surface of the GCA, which can explain the fact that the sulfate ion concentration in the GCA bottles increased as shown in **Fig. 1**. The oxidation of sulfides by manganese oxide was also observed in natural systems [17, 18].

The titanium K edge spectra of GCA did not change between the initial and the final GCA (**Fig. 7**). Moreover, the TiS_3 adsorption edge was higher than that of GCA, indicating that TiS_3 were not formed on the GCA (**Fig. 7**). Considering titanium XANES, titanium contained in GCA does not play an important role in hydrogen sulfide removal.

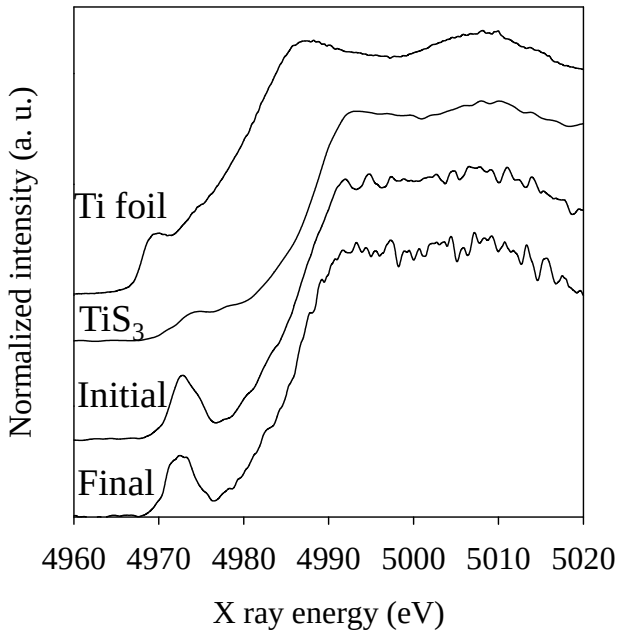

Fig. 7

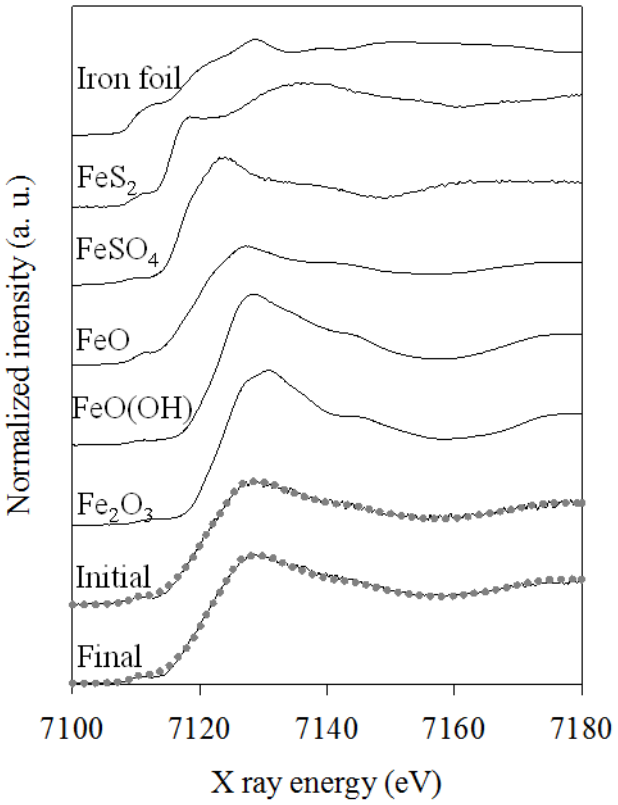

Fig. 8

The iron K edge spectra of the initial and the final GCA are shown in **Fig. 8**. The FeS_2 (pyrite) has lower adsorption edge compared to that of the GCA. Eh-pH diagram of iron shows pyrite is not formed thermodynamically in this study since pyrite is formed under much lower Eh conditions (**Fig. 9**). The iron K edge spectra of GCA can be successfully fit by a combination of FeO, Fe_2O_3 (hematite) and iron hydroxide ($Fe^{III}O(OH)$) (**Fig.8**). It is reasonable to fit these standards since the FeO and Fe_2O_3 can thermodynamically represent the iron components of coal ash [19]. Under reducing condition, FeO is formed at around 1,173 K due to the decomposition of hematite [20]. Iron hydroxide (III) might be partially formed on the surface of the GCA

through hydrolysis. Fractions of iron species of the initial and the final GCA were calculated by curve fitting (**Table 2**). Comparing initial and final adsorption of hydrogen sulfide, hematite contents did not significantly change, while FeO was partially oxidized to iron hydroxide (III). Unlike manganese, iron was not reduced by hydrogen sulfide. As shown in **Fig. 9**, the hematite is considered to be the thermodynamically most stable iron species under the present experimental conditions.

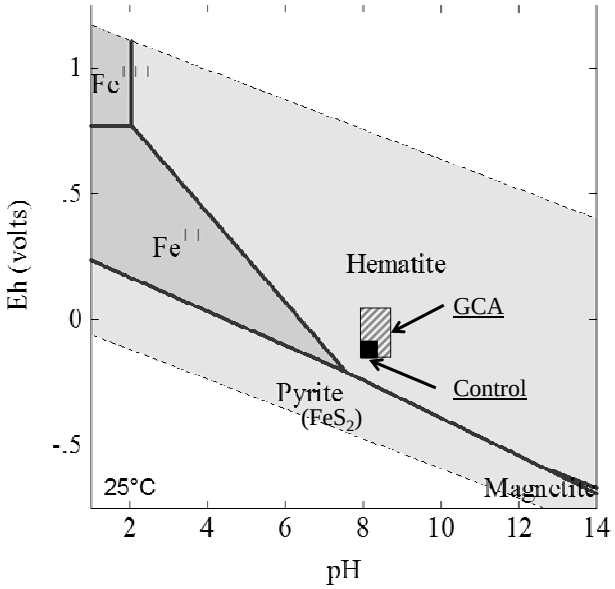

Fig. 9

It is well known that the main edge shifts to higher energy with increased oxidation state. As previously mentioned, pyrite and iron sulfide were not formed on the GCA. Besides, the iron absorption K edge and the main peak of $FeSO_4$ were lower than those of GCA (**Fig. 8**). Therefore, in this study, we discussed iron K edge of GCA on the basis of iron oxides. Iron K edge shifted to higher energy region with increased oxidation state (**Table 3**). The iron K edge of the initial and the final GCA were 7119.5 and 7120.9 eV, respectively.

The absorption edge was very close to that of ferrous oxide. This result corresponds well with the fitted curve results indicating that the ferrous iron is the major iron species on the GCA. Thus, most of the iron contained in the GCA is not easily reduced by hydrogen sulfide since it requires a strong reducer such as sodium tetrahydroborate to reduce ferrous iron to zero valent iron [21]. Therefore, iron in the GCA does not also play an important role in hydrogen sulfide removal.

To summarize the XAFS analyses, the sulfides were not formed on the GCA, instead hydrogen sulfide was oxidized to sulfur, sulfite and sulfate. The sulfur K edge XANES of the final GCA with different amounts of hydrogen sulfide adsorption could be well fitted by the sulfur and sulfite standards and sulfate originating from the initial GCA (**Fig. 4**). Sulfur species of the final GCA was calculated (**Table 4**), showing that percent composition of sulfur increased with increasing amount of hydrogen sulfide adsorption. Therefore, the major reaction is the oxidation of hydrogen sulfide to sulfur. In natural systems, hydrogen sulfide is oxidized to sulfur by MnO_2 [17, 18]. In the case with the GCA, the oxidized reaction is assumed as Eq. (2) under the reduced condition.

$$Mn_2O_3 + H_2S + 4H^+ = 2Mn^{2+} + S + 3H_2O \quad \cdots \quad (2)$$

Although Eq. (2) is a major reaction, the sulfate ion concentration increased in the GCA and the presence of $MnSO_4$ on the GCA was observed as well (**Figs.1 and 5**). Hence, the sulfur might be partially oxidized to sulfate on the surface of the GCA.

4. Conclusions

Combined adsorption and oxidation mechanisms of hydrogen sulfide on granulated coal ash were revealed in this study. Hydrogen sulfide was adsorbed onto the GCA and successively oxidized to sulfur and partially to sulfate by manganese oxide contained in the GCA.

Acknowledgements

Experiments at HiSOR were carried out under the approval of the HSRC Program Advisory Committee (#:08-A-34 and #10-A-01). XAFS analyses carried out at the Ritsumeikan SR Center under the approval of the "Nanotechnology Network Japan Program" (S23-15).

References

[1] Y. Xiao, S. Wang, D. Wu and Q. Yuan, Separ. Purif. Technol. 59 (2008) 326-332.

[2] K. T. Li and W. D. Cheng, Appl. Catal. A: General 142 (1996) 315-326.

[3] N. Rakmak, W. Wiyaratn, C. Bunyakan and J. Chungsiriporn, Chem. Eng. J. 162 (2010) 84-90.

[4] M. I. Kim, D.W. Park, S.W. Park, X. Yang, J.S. Choi and D.J. Suh, Catal. Today 111 (2006) 212-216.

[5] N. Haimour, R. E. Bishtawi and A. A. Wahbi, Desalination 181 (2005)145-152.

[6] T. D. Nguyen, K. Block and T. J. Bandosz, Chemosphere 59 (2005) 343-353.

[7] JCOAL, Japan Coal Energy Center, http://www.jcoal.or.jp/coalash/pdf/CoalAsh_H19productiondata.pdf (in

Japanese) (accessed on 30.11.2011).

[8]S. Asaoka, T. Yamamoto and S. Hayakawa, J. Japan Soc. Wat. Environ. 32 (2009) 363-368. (in Japanese with English abstract)

[9]S. Asaoka, T. Yamamoto, I. Yoshioka and H. Tanaka, J. Hazard. Mater. 172 (2009) 92-98.

[10]S. Asaoka, T. Yamamoto and K. Yamamoto, J. Japan Soc. Wat. Environ. 31 (2008) 455-462. (in Japanese with English abstract).

[11] APHAAWWAWEF, Standard Method for the Examination for Water and Wastewater 18th ed., American Water Works Association, Water Environment Federation, Baltimore, MD., 1992, pp. 2-60.

[12] K. Ito, in: Samukawa, S. and Hiiro, K. (Eds.), Gihodo, Tokyo, 1996, pp. 93.(in Japanses).

[13] S. Hayakawa, Y. Hajima, S. Qiao, H. Namatame and T., Hirokawa, Anal. Sci. 24 (2008) 835-837.

[14]L. Backnaes, J. Stelling, H. Behrens, J. Goettlicher, S. Mangold, O. Verheijen, R. G. C. Beerkens and J. Deubener, J. Am. Ceram. Soc. 91 (2008)721-727.

[15] S. Matsumoto, Y. Tanaka, H. Ishii, T. Tanabe, Y. Kitajima and J. Kawai, Spectrochim. Acta B 61 (2006) 991-994.

[16] M.E. Fleet, S.L. Harmer, X. Liu and H.W. Nesbitt, Surf. Sci. 584 (2005)133-145.

[17] W. Yao and F. J. Millero, Geochim. Cosmochim. Acta 57 (1993) 3359-3365.

[18]B. Thamdrup, H. Fossing and B.B. Jørgensen, Geochim. Cosmochim. Acta 58 (1994) 5115-5129.

[19] E. Jak, S. Degterov, P. C. Hayesand and A. D. Pelton, Fuel 77 (1998) 77-84.

[20] Z. Zhang, X. Wu, T. Zhou, Y. Chen, N. Hou, G. Piao, N. Kobayashi, Y.

Itaya and S. Mori, Proc. Combust. Ins. 33 (2011) 2853-2861.

[21] R. J. Barnes, O. Riba, M. N. Gardner, T. B. Scott, S. A. Jackman and I. P. Thompson, Chemosphere 79 (2010)448-454.

Figure captions

Fig. 1 Time course concentrations of hydrogen sulfide and sulfate ion
(A): Initial concentration: 8 mg-S L^{-1}; (B): Initial concentration: 85 mg-S L^{-1}

Fig. 2 Time course of pH and Eh
(A): Initial concentration: 8 mg-S L^{-1}; (B): Initial concentration: 85 mg-S L^{-1}

Fig. 3 Contributions for hydrogen sulfide removal
(A): Initial concentration 8 mg-S L^{-1}; (B): Initial concentration 85 mg-S L^{-1}
C: Control; G: GCA

Fig. 4 Sulfur K edge XANES spectra of the GCA and several sulfur standards
Standard of Al_2S_3, CaS and FeS are refered to Asaoka et al., 2009 [8]. The black curves and gray dotted curves are observed spectra and curve fitting results, respectively. Initial is GCA without hydrogen sulfide adsorption; The value of 1.5, 9.5, 18 mg g^{-1} are amount of hydrogen sulfide adsorbed onto the GCA

Fig. 5 Manganese K edge XANES spectra of the GCA and several manganese standards
The black curves and gray dot curve are observed spectra and curve fitting result, respectively. Initial is the GCA without hydrogen sulfide adsorption; Final is the GCA with hydrogen sulfide adsorption

Fig. 6 Eh-pH diagram of manganese
The shaded area and black filled area are the batch experiment conditions

Fig. 7 Titanium K edge XANES spectra of the GCA and titanium standards
Initial is the GCA without hydrogen sulfide adsorption; Final is the GCA with hydrogen sulfide adsorption

Fig. 8 Iron K edge XANES spectra of GCA and several iron standards
Initial is the GCA without hydrogen sulfide adsorption; Final is the GCA with hydrogen sulfide adsorption; The black curves and gray dotted curves

are observed spectra and curve fitting results, respectively.

Fig. 9 Eh-pH diagram of iron
The shaded area and black filled area are the batch experiment conditions

Figures

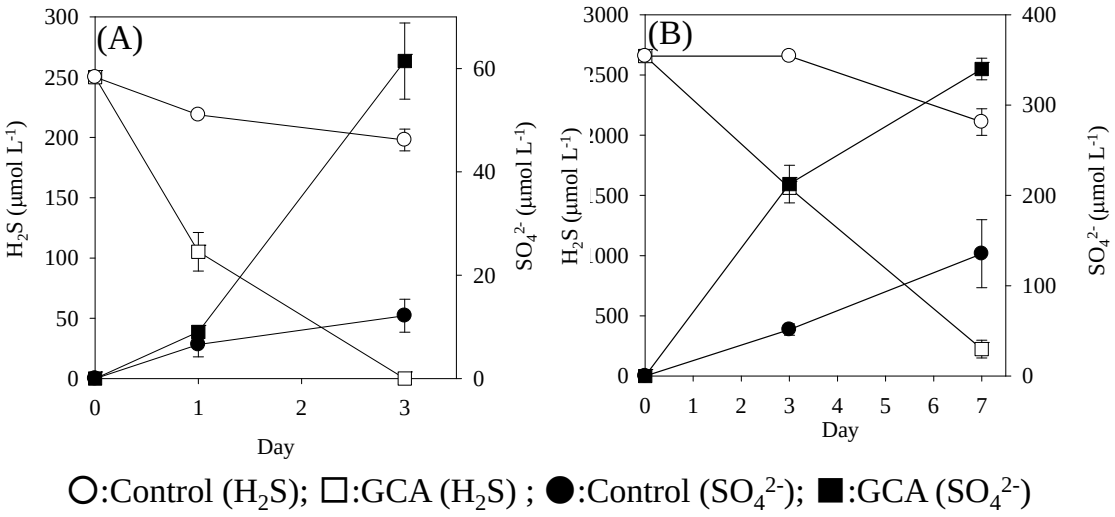

Fig. 1

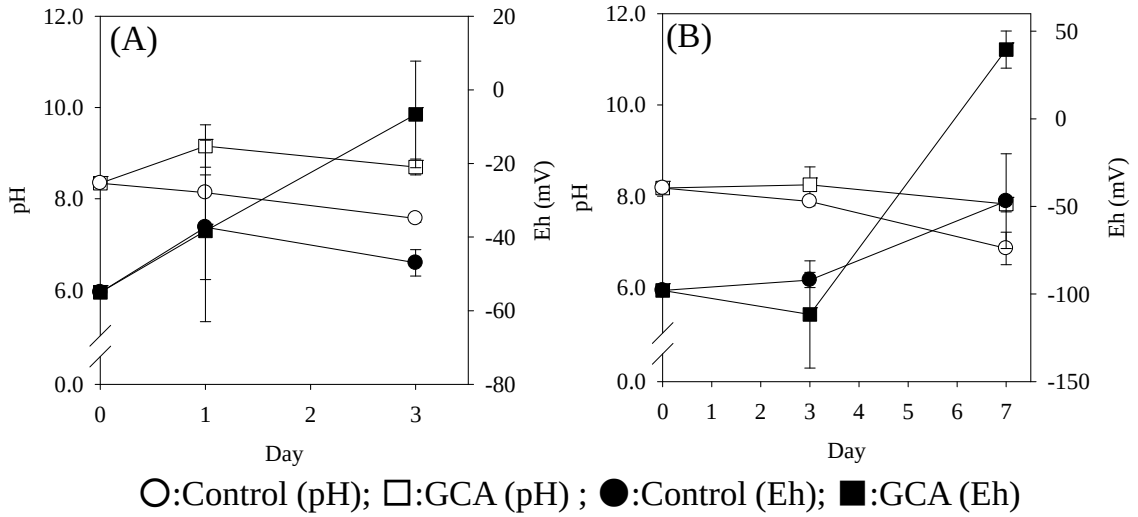
(A)
(B)
pH
Eh (mV)
Day
12.0
10.0
8.0
6.0
0.0
20
0
-20
-40
-60
-80
50
-50
-100
-150
0 1 2 3 4 5 6 7
○:Control (pH); □:GCA (pH) ; ●:Control (Eh); ■:GCA (Eh)

Fig. 2

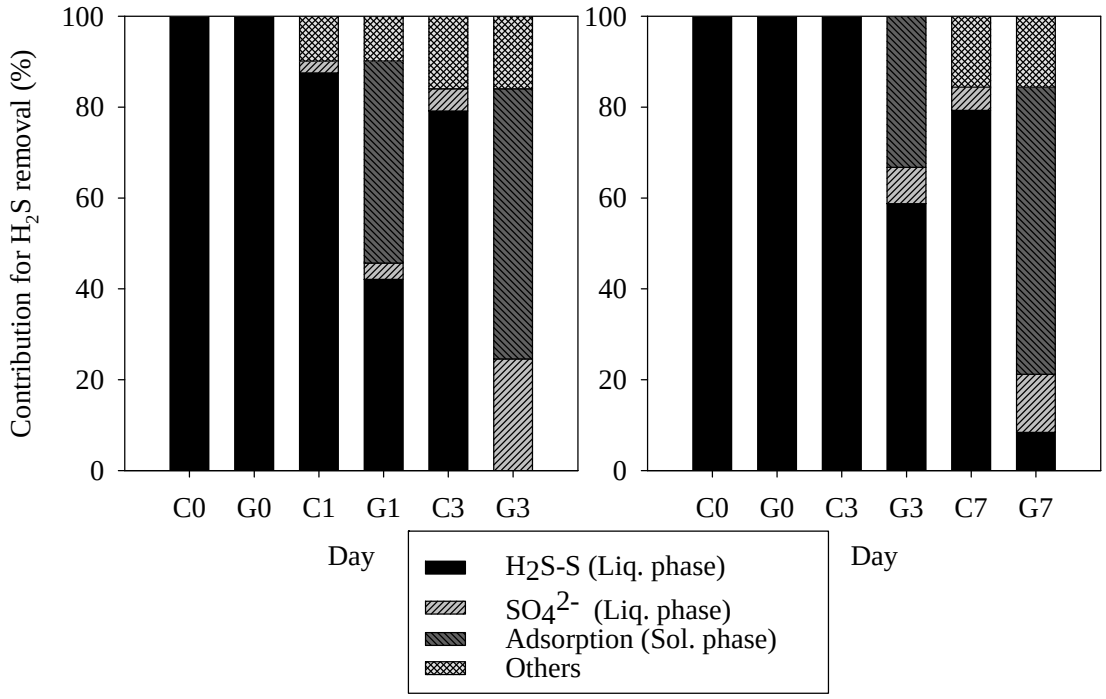
Contribution for H_2S removal (%)
100
80
60
40
20
0
C0
G0
C1
G1
C3
G3
Day
C0
G0
C3
G3
C7
G7
Day
H_2S-S (Liq. phase)
SO_4^{2-} (Liq. phase)
Adsorption (Sol. phase)
Others

Fig. 3

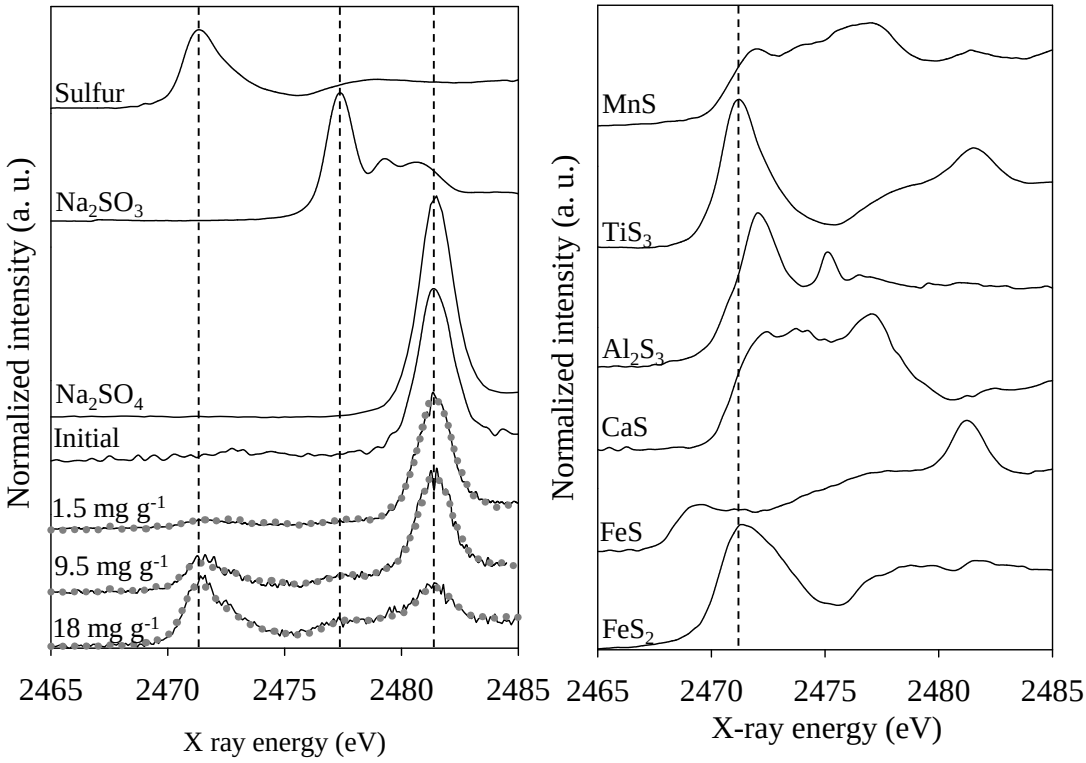
Sulfur
Na2SO3
Na2SO4
Initial
1.5 mg g-1
9.5 mg g-1
18 mg g-1
Normalized intensity (a. u.)
2465
2470
2475
2480
2485
X ray energy (eV)
MnS
TiS3
Al2S3
CaS
FeS
FeS2
Normalized intensity (a. u.)
2465
2470
2475
2480
2485
X-ray energy (eV)

Fig. 4

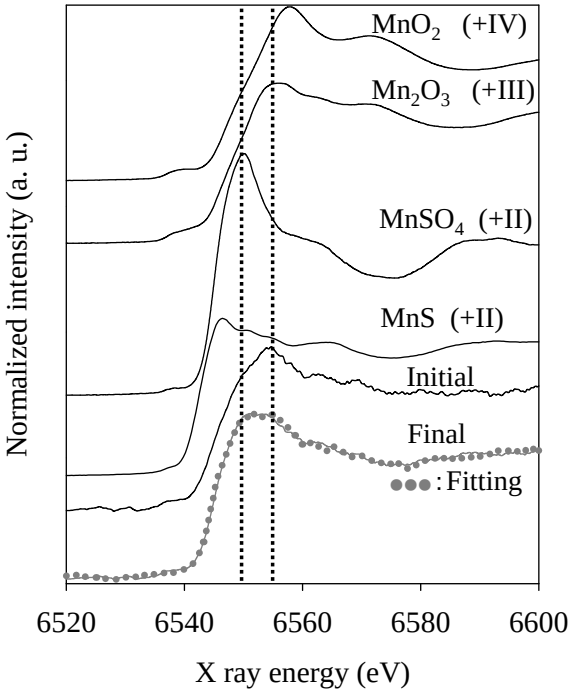
MnO2 (+IV)
Mn2O3 (+III)
MnSO4 (+II)
MnS (+II)
Initial
Final
●●●: Fitting
Normalized intensity (a. u.)
6520
6540
6560
6580
6600
X ray energy (eV)

Fig. 5

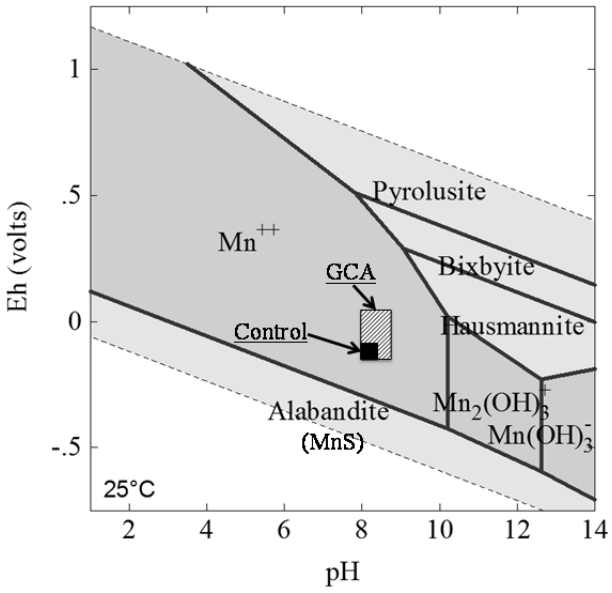
1
.5
0
-.5
Eh (volts)
Mn++
Pyrolusite
Bixbyite
Hausmannite
GCA
Control
Alabandite
(MnS)
Mn2(OH)+6
Mn(OH)-3
25°C
2
4
6
8
10
12
14
pH

Fig. 6

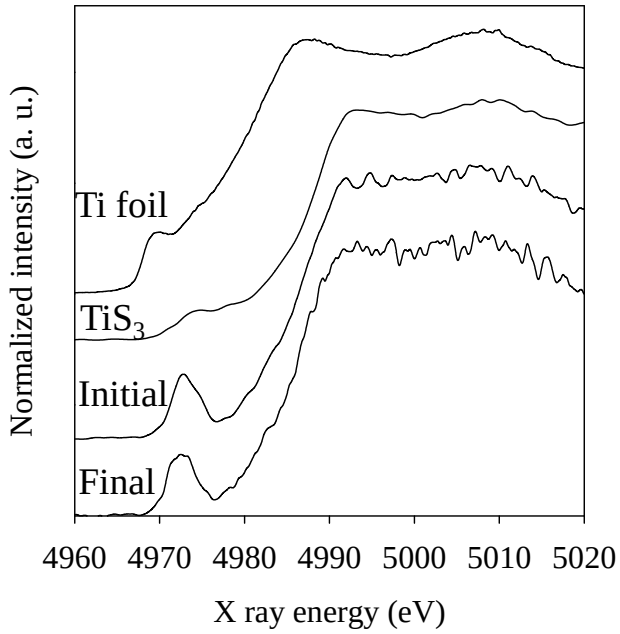
Normalized intensity (a. u.)
Ti foil
TiS3
Initial
Final
4960
4970
4980
4990
5000
5010
5020
X ray energy (eV)

Fig. 7

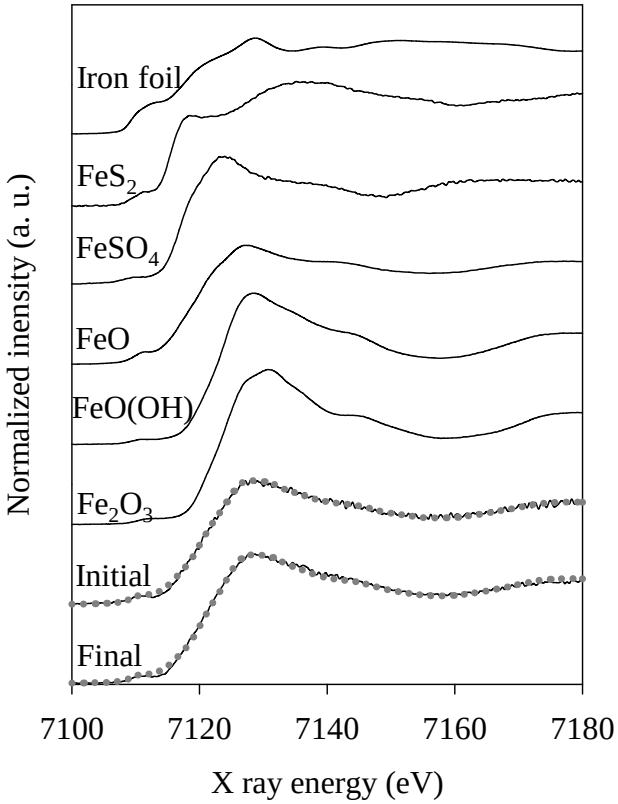
Iron foil
FeS2
FeSO4
FeO
FeO(OH)
Fe2O3
Initial
Final
Normalized inensity (a. u.)
7100
7120
7140
7160
7180
X ray energy (eV)

Fig. 8

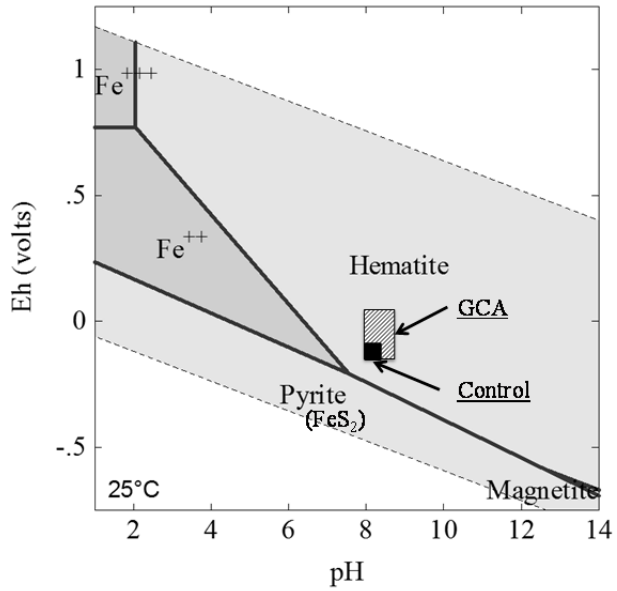
Eh (volts)
1
.5
0
-.5
Fe+++
Fe++
Hematite
GCA
Control
Pyrite
(FeS2)
25°C
Magnetite
2
4
6
8
10
12
14
pH

Fig. 9

Tables

Table 1 Chemical composition of granulated coal ash

Main elements (g/kg-dw)		Trace elements (mg/kg-dw)			
SiO_2	395.3	Ba	397	Rb	28.8
CO_3^{2-}	133	MnO	329	Co	28.6
Al_2O_3	125.5	Zr	298	Cr	27.2
CaO	55.4	N	200	Ga	20.6
C	27.4	V	111	Nb	34.4
Fe_2O_3	22.5	Zn	88.9	Sc	14.5
MgO	8.11	Ce	69.7	Th	12.7
K_2O	6.09	Cu	58.9	Hf	6.7
H	5.2	Y	52.6	W	5.2
TiO_2	5.68	Nd	34.4	U	4.2
Na_2O	2.5	La	34.2	Yb	3.9
P_2O_5	1.86	Pb	29.3	Cs	3.2
Sr	0.4	Ni	29.2		

(Asaoka et al., 2008)[10]

Table 2 Fraction of iron species in the GCA derived from the curve fitting of the Fe K-edge XANES spectra

Iron species	Initial (%)	Final(%)
FeO	64	56
Fe_2O_3	30	33
FeO(OH)	6	11

Table3 Iron K absorption edge of GCA and several iron standards

Iron species	Valence	Absorption edge (eV)
Iron foil	0	7109.7
FeO	+II	7119.5
FeO(OH)	+III	7123.2
Fe_2O_3	+III	7123.2
Initial GCA	-	7119.5
Final GCA	-	7120.9

Table 4 Fraction of sulfur species in the GCA with different amounts of hydrogen sulfide adsorption evaluated from the curve fitting of S K-edge XANES spectra

Amount of adsorbed (mg/g)	Fraction (%)		
	Sulfate	Sulfite	Sulfur
0	100	0	0
1.5	89	3	8
9.5	63	4	33
18	21	4	75